

# Some Properties of an Axisymmetric Pulsar Magnetosphere Constructed by Numerical Calculation

Jun OGURA and Yasufumi KOJIMA

*Department of Physics, Hiroshima University, Higashi-Hiroshima 739-8526, Japan*

(Received October 16, 2002)

We have explored the magnetosphere described by a numerical solution for an axisymmetric rotating field satisfying the force-free and ideal MHD conditions everywhere. The electric current distribution is determined by the requirement of continuity and smoothness of the flux function across the light cylinder. The overall magnetic field structure is obtained using the numerical result. We also checked the drift velocity of a charged particle, which is caused by the resultant electric and magnetic fields. It is found that the velocity exceeds the light speed beyond a few times the size of the light cylinder. This fact suggests the breakdown of some underlying assumptions.

## §1. Introduction

It is well known that rotating magnetized neutron stars emit radiation from radio waves to gamma rays, and constitute a power supply to surrounding nebula. The basic idea of a pulsar was proposed more than 30 years ago (e.g., Refs. 1) and 2)), but a detailed consistent model has not yet been constructed. Almost all the energy is carried out from a pulsar by electromagnetic fields, but it is converted to particle kinetic energy at large distances.<sup>3)</sup> Several authors have discussed the conversion mechanisms, such as non-ideal MHD effects,<sup>4)</sup> magnetic reconnection<sup>5),6)</sup> and plasma instability.<sup>7),8)</sup> Because the dissipation of electro-magnetic fields is related to the acceleration of particles, and hence the observed radiation, the determination of the mechanism is very important.

The global structure of the magnetosphere, even without dissipation, is not easily determined. The configuration is strongly coupled with the plasma flow. Several authors have used simplified electromagnetic models, such as a monopole magnetic field, to investigate the plasma dynamics. For instance, Michel<sup>9),10)</sup> considered cold MHD winds for an aligned pulsar, and Bogovalov<sup>11)</sup> extended it to the oblique case. The monopole magnetic field itself is unrealistic, but some results may be used as a model of pulsar magnetosphere. It is desirable to consider the plasma dynamics with a more realistic magnetic field, e.g., a dipole field near the star. We may gradually confirm the existing general picture, or we may find incorrect aspects of previous models, using a realistic model.

The pulsar equation determines an axially symmetric MHD field in the force-free limit (e.g., Refs. 14),13),12)). Recently, Contopoulos et al.<sup>15)</sup> obtained a new type of numerical solution of the pulsar equation. We refer to their solution as the CKF solution in this paper. Their solution represents the interesting structure that the magnetic field is a dipole near the star and asymptotically approaches a

split-monopole form at far distances. Their results also show that the solution is smooth across the light cylinder, and there is no evidence of a singularity of the flow and field. In a subsequent paper,<sup>16)</sup> Contopoulos and Kazanas proposed a possible conversion mechanism of pulsar power into particle energy in the wind region, using their solution.

For the above reason, the CKF solution is quite interesting. In particular, the non-singular property is *in stark contrast with the previous understanding* that a dissipation-free flow would lead to a singularity in the flow and the magnetic field, occurring a short distance beyond the light cylinder (e.g., Ref. 4)). The drift approximation is expected to break down near the light cylinder (e.g., Ref. 13)), since the drift velocity  $|\vec{v}_\perp| = c|\vec{E} \times \vec{B}|/B^2$  approaches the light speed  $c$  due to the fact that  $|E| \sim |B|$  in the wind region. These arguments sound reasonable, but depend strongly on the electro-magnetic field configuration. If there were no drawbacks of the CKF solution, it would allow for the understanding of the pulsar magnetosphere to progress significantly, or it would reveal the need to change the current picture presented in the literature.<sup>4),13)</sup> On the other hand, if the validity of the CKF solution could be checked, this solution could be used as the lowest approximation, and various physical effects could be added to it. Furthermore, it would help to understand other astrophysical phenomena, because the pulsar equation can also be applied to the black hole magnetosphere and jets (e.g., Ref. 14)). Therefore, it is quite important to determine the properties of the CKF solution.

The purpose of this paper is to explore the physical quantities described by the CKF solution. In particular, we explicitly calculate the electro-magnetic structure and drift velocity. These quantities were not given in Ref. 15). We calculated them by differentiating the magnetic flux function. For the numerical differentiation, it was necessary to construct a flux function using many more grid points than in the computation reported in Ref. 15). Furthermore, the validity of the CKF solution is investigated. In §2, we briefly summarize the basic equations for the axially symmetric MHD field in the force-free limit. In §3, we briefly summarize the numerical method and the CKF solution constructed using numerical calculations. In §4, the magnetic field structure and drift velocity are calculated. Finally, some remarks are given in §5. In the appendix, we also briefly summarize some properties of the split-monopole magnetic field, which can be calculated analytically, and is useful for comparison.

## §2. Assumptions and formalism

In this section we briefly summarize the equations governing the stationary axisymmetric magnetosphere. In the axisymmetric case, it is convenient to decouple the poloidal and toroidal parts of the magnetic fields in cylindrical coordinates,  $(R, \phi, Z)$ . The poloidal field  $\vec{B}_p = (B_R, B_Z)$  is written in terms of the flux function  $\Phi(R, Z)$ , while the toroidal field is given by another function,  $A(R, Z)$ , as

$$(B_R, B_\phi, B_Z) = \left( -\frac{1}{R} \partial_Z \Phi, \quad \frac{1}{R} A, \quad \frac{1}{R} \partial_R \Phi \right). \quad (2.1)$$

On the basis of some assumptions, the function  $A$  should depend only on  $\Phi$ , as discussed below. The plasma is assumed to be frozen to the magnetic field everywhere. In the limit of large magnetic Reynolds number, the velocity component perpendicular to the magnetic field is described by the so-called “ $E \times B$ ” drift velocity,

$$\vec{v}_\perp = \frac{c\vec{E} \times \vec{B}}{B^2}. \quad (2.2)$$

Including the velocity along the magnetic field line, the electric and magnetic fields satisfy the relation

$$\vec{E} + \frac{\vec{v}}{c} \times \vec{B} = 0. \quad (2.3)$$

This condition holds if there exists a sufficient amount of charge density, whose origin is discussed in the literature.<sup>13), 12)</sup>

As a first step to understanding the overall structure without a realistic dissipation mechanism, we here ignore the small gap regions and consider the electromagnetic structure on a much larger length scale. From the ideal MHD condition (2.3), the electric field can be expressed by

$$(E_R, E_\phi, E_Z) = \left( -\frac{\Omega}{c} \partial_R \Phi, 0, -\frac{\Omega}{c} \partial_Z \Phi \right) = -\vec{\nabla} \left( \frac{\Omega}{c} \Phi \right), \quad (2.4)$$

where the angular velocity of the magnetic field line  $\Omega$  is also a function of  $\Phi$  in general, but we assume it to be constant in this paper. Therefore, the magnetosphere rotates like a rigid body.

The charge density  $\rho_e$  is given by the divergence of the electric field (Gauss's law), and the current  $\vec{j}$  by the rotation of the magnetic field (Ampere's law). They are explicitly written as

$$\rho_e = -\frac{\Omega}{4\pi c} \Delta \Phi = -\frac{\Omega}{4\pi c} \left( \frac{1}{R} \partial_R R \partial_R \Phi + \partial_Z^2 \Phi \right), \quad (2.5)$$

$$(j_R, j_\phi, j_Z) = \frac{c}{4\pi} \left( -\frac{1}{R} \partial_Z A, -\frac{1}{R} \left( \Delta \Phi - \frac{2}{R} \partial_R \Phi \right), \frac{1}{R} \partial_R A \right). \quad (2.6)$$

We assume that the electro-magnetic force dominates. That is, we ignore the gravity, pressure and the inertial terms. The force-free condition is written

$$\rho_e \vec{E} + \frac{\vec{j}}{c} \times \vec{B} = 0. \quad (2.7)$$

After some algebra, we find that the function  $A$  is on a surface of constant  $\Phi$ , i.e.  $A = A(\Phi)$ . The function  $\Phi$  should satisfy the so-called ‘pulsar equation’,

$$(1 - \beta^2) \Delta \Phi - \frac{2}{R} \partial_R \Phi + A A' = 0, \quad (2.8)$$

where  $\beta$  is the cylindrical radius normalized with respect to the light cylinder:  $\beta = R\Omega/c = R/R_{LC}$ . Using Eq. (2.8), the current and charge density can be rewritten

as

$$(j_R, j_\phi, j_Z) = \frac{c}{4\pi} \left( A' B_R, -\frac{1}{R} \frac{2\beta^2 B_Z - AA'}{1 - \beta^2}, A' B_Z \right), \quad (2.9)$$

$$\rho_e = -\frac{\Omega}{4\pi c} \frac{2B_Z - AA'}{1 - \beta^2}. \quad (2.10)$$

The current flow within the flux tube  $\Phi$  is given by

$$J(\Phi) = \int_0^\Phi \vec{j} \cdot d\vec{S} = \int_0^\Phi \frac{1}{4\pi R} A' |\nabla \Phi| \frac{2\pi R d\Phi}{|\nabla \Phi|} = \frac{c}{2} A(\Phi), \quad (2.11)$$

where we have defined  $\Phi = 0$  as the  $Z$ -axis. Therefore,

$$A(0) = 0 \quad (2.12)$$

is obtained from the regularity of the toroidal magnetic field (see §3).

### §3. Numerical scheme to solve the singular equation

#### 3.1. Boundary conditions

The pulsar equation (2.8) is seen to have a singular surface, i.e. the light cylinder  $R = R_{LC} = c/\Omega$ . Both inside and outside the light cylinder, the equation becomes a partial differential equation of the elliptic type for a given function  $A$ . The procedure for constructing a numerical solution of (2.8) is to solve the equation on each side and to match the solutions at the light cylinder. The interior and exterior solutions are not in general continuous across the light cylinder for an assumed function  $A$ . Therefore, the function  $A$  should be modified iteratively so as to converge.

We set boundary conditions for the elliptic equation that are almost the same as for the CKF solution. The function  $\Phi$  near the star is described by a dipole magnetic field with magnetic dipole moment  $m$  as

$$\Phi = \frac{mR^2}{(R^2 + Z^2)^{3/2}}. \quad (3.1)$$

The last open field line for this dipole field corresponds to  $\Phi = \Phi_{pc} \equiv m/R_{LC}$ , which passes the light cylinder on the equatorial plane. At the polar axis,  $\Phi$  is given by the Dirichlet condition as

$$\Phi(0, Z) = 0. \quad (3.2)$$

The boundary condition at the outer right points is given by the Neumann condition as

$$\partial_R \Phi(R_{\max}, Z) = 0, \quad (3.3)$$

while, the upper outermost boundary is given by

$$\Phi(R, Z_{\max}) = 0, \quad (3.4)$$

where the domain of calculation is limited to  $0 \leq R \leq R_{\max}$ ,  $0 \leq Z \leq Z_{\max}$ . The conditions  $R_{\max} = \infty$  and  $Z_{\max} = \infty$ , were applied to the CKF solution, using a certain coordinate transformation, but we limited the spatial domain as  $R_{\max} = Z_{\max} = 9R_{LC}$ . The effect of this change was numerically checked, and we found that there is no substantial difference between the results obtained in the two cases. Our choice is better to facilitate numerical convergence. We also changed the outer boundary conditions, but we found that they are not so sensitive to the boundary conditions, and the calculations converge to the result almost uniquely. The boundary condition on the equatorial plane is divided by the light cylinder. Because particles can rotate with the star within the light cylinder, we have

$$\partial_Z \Phi(R, 0) = 0. \quad (R \leq R_{LC}) \quad (3.5)$$

Outside the light cylinder, the line is extended to infinity. We therefore set it as

$$\Phi(R, 0) = \Phi_{\text{open}}, \quad (R > R_{LC}) \quad (3.6)$$

where  $\Phi_{\text{open}}$  is the last inner open field line, i.e.  $\Phi(R_{LC}, 0)$  calculated for the interior solution.

In order to avoid the singular surface of Eq. (2.8), we require at the light cylinder  $R = R_{LC} = c/\Omega$  the relation

$$AA' = \frac{2}{R} \partial_R \Phi = 2B_Z. \quad (3.7)$$

In this case, the singularities of the charge density  $\rho_e$  and toroidal current  $j_\phi$  vanish simultaneously [See Eqs. (2.9)–(2.10).]

It is not clear *a priori* which functional form of  $A(\Phi)$  satisfies all of the boundary conditions. We therefore need to carry out an iterative process to obtain the solution. Contopoulos et al.<sup>15)</sup> successfully solved the equation by searching for a suitable function  $A$  so as to match the interior and exterior solutions at the surface. We used the same relaxation-type technique.

### 3.2. Results

We solved Eq. (2.8) with the boundary conditions in the numerical domain  $R_{\max} = Z_{\max} = 9R_{LC}$ . A self-consistent solution for  $\Phi$  and  $A(\Phi)$  was calculated on a grid with  $80 \times 80$  points inside and another  $80 \times 80$  points outside the light cylinder to insure numerical accuracy. The calculation required more than  $10^4$  iterations to realize a smooth result. We performed many trials to search for different types of solutions, but just one, the CKF solution, was found. This may be a unique solution satisfying the boundary conditions, although we have not yet proved this. The overall structure of the solution is the same as that of the CKF solution, but the value of the last open field line is a little bit larger than that of the actual CKF result. The result in that case, obtained with a  $30 \times 30$  grid, is  $\Phi_{\text{open}} = 1.36\Phi_{pc}$ , while our result is  $\Phi_{\text{open}} = 1.66\Phi_{pc}$ . The origin of this discrepancy is presumably the difference in numerical resolution. (We used more than twice as many grid points in each direction.) We also checked their result with a calculation using a  $30 \times$

30 grid. We found that the value  $\Phi_{\text{open}}$  increases slightly with the grid points, but our numerical result seems to converge to a value around  $\Phi_{\text{open}} = 1.66\Phi_{pc}$ . It is interesting to compare this value with that for the case of constant  $A$ ,<sup>10)</sup> in which  $\Phi_{\text{open}} = 1.592\Phi_{pc}$ . The precise value depends on the numerical accuracy, and scales the physical quantities of the solution. The calculated function  $\Phi(R, Z)$  is shown in Fig. 1. Both interior and exterior functions connect smoothly across the light cylinder. We only show the result for the inner part of the numerical calculation, where  $0 \leq R/R_{LC} \leq 4$ ,  $0 \leq Z/R_{LC} \leq 3$ . The result in this region is almost unaffected by our choice of the outermost boundary conditions at  $R_{\text{max}}$ ,  $Z_{\text{max}}$ .

The function needed during the numerical iterations is not  $A$ , but  $AA'$ . The conditions adopted in our numerical calculation are  $AA' = 0$  for  $\Phi = 0$  and  $\Phi \geq \Phi_{\text{open}}$ , where we used Eq. (2.12) and the implicit assumption that the electric circuit is closed in the whole system:

$$A(\Phi) = 0. \quad (\Phi \geq \Phi_{\text{open}}) \quad (3.8)$$

The function  $A$  is constructed from the numerical data for  $AA'$ . The result is shown in Fig. 2. The result indeed shows that  $A(\Phi_{\text{open}}) \neq 0$ . This causes serious problems when applying our computation to physical situations. The current closure is not realized, and there is a discontinuity of  $B_\phi$  in this model. The total current from the upper hemisphere has a definite sign,  $J < 0$ . A simple way to use this model is to introduce a thin current sheet on  $\Phi_{\text{open}}$ . This artificially ensures that a return current sheet equal to  $-A(\Phi_{\text{open}})$  flows along the equatorial plane ( $R > R_{LC}$ ) and the last open field line. The discontinuity of  $B_\phi$  on  $\Phi_{\text{open}}$  is clear, because  $B_\phi \neq 0$  along the open field line, and  $B_\phi = A(\Phi)/R = 0$  on the closed line. This discontinuity may be related to the current sheet. However, in a model with the current sheet, an enormously strong force, such as that due to a pressure, would be required.

One may think that a stringent condition, such as  $A = 0$  at  $\Phi = 0$  and  $\Phi_{\text{open}} = 0$ , should be imposed in order to construct a more realistic model (without an artificial current sheet). We used this condition in the numerical iteration, but we did not obtain a convergent solution. Our numerical experiment may not be complete, but it suggests that a global solution of the pulsar equation can be obtained only under the weak conditions on  $A$  used in previous works.<sup>15)</sup>

We also compared the functional form of our result with that in the split-monopole case. The interesting point regarding the CKF solution is the existence of separated regions with different signs of  $A'$ . The poloidal current flows along a constant  $\Phi$  surface, and the current in the interval  $d\Phi$  is  $dJ = cA'd\Phi/2$ . The region in which  $A' < 0$  ( $0 \leq \Phi < 1.36\Phi_{pc}$ ) corresponds to an out-flowing electron (or an in-flowing positron), and that in which  $A' > 0$  ( $1.36\Phi_{pc} < \Phi \leq \Phi_{\text{open}}$ ) corresponds to an in-flowing electron. However, the amount of flow in the region satisfying  $A' > 0$  in this model is insufficient to satisfy the current closure condition,  $J = 0$ .

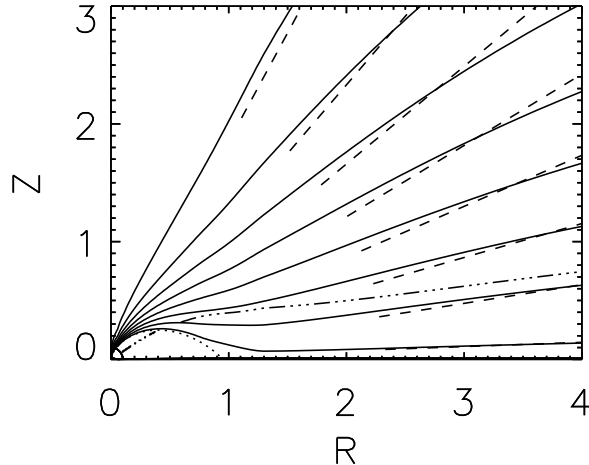


Fig. 1. Structure of the axisymmetric force-free magnetosphere of an aligned rotating magnetic dipole. The solid curves represent the flux surfaces in intervals of  $0.2\Phi_{pc}$ , with  $\Phi = 0$  along the axis, while dashed curves represent those of the split-monopole solution. The dotted curve represents the last open field line,  $\Phi_{open} = 1.66\Phi_{pc}$ . The boundary condition near the star is imposed at the quarter circle indicated in the lower left-hand corner of the figure. The dotted-dash curve indicates the null surface.

#### §4. Properties of the CKF solution

##### 4.1. Global magnetic field structure

In Fig. 3, we display the magnetic fields derived from the numerical solution. The field strength of each component is represented by the contours. We also show the magnetic fields for the split-monopole solution for comparison. One obviously different region is inside the last closed line. The overall magnetic field structure is almost the same, except in certain regions. This seems reasonable, since the difference between the fields in the functions  $\Phi$  and  $A$  is not so large, as shown in §3.

We now consider the differences in detail. For  $B_R$  of the CKF solution, there exists a discontinuity on the equatorial plane around  $(R_{LC}, 0)$ . This behavior results from the boundary condition on the equatorial plane. As described in §3, the numerical boundary conditions are divided by the point  $(R_{LC}, 0)$ . The condition inside the light cylinder ensures  $B_R = 0$  on the equatorial plane and  $B_R \neq 0$  in general outside the light cylinder. Therefore, it might be a subtle problem to devise a proper numerical treatment around the point  $(R_{LC}, 0)$ .

Constructing numerical treatment around the  $Z$ -axis may also be subtle. In the numerical calculation, we imposed the condition  $A \rightarrow 0$  as  $\Phi \rightarrow 0$  (i.e. as  $R \rightarrow 0$ ),

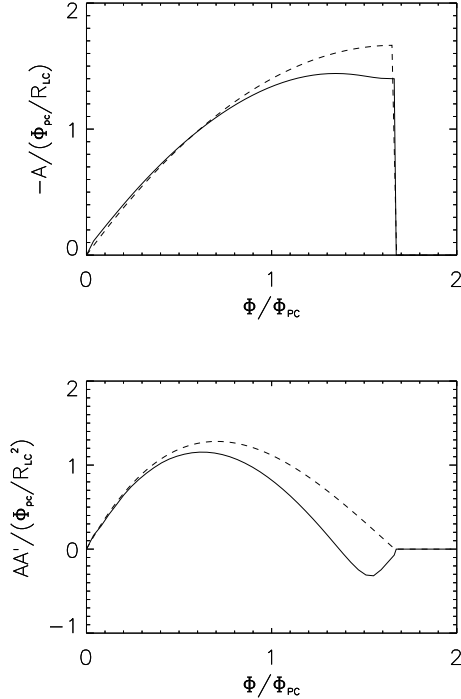


Fig. 2. The electric current distribution along open field lines. The solid curve represents our numerical results. It is similar to the CKF solution, but is stretched to larger values of  $\Phi_{pc}$ . The dotted curve represents the results for the split-monopole solution.

but we have to determine the value  $B_\phi = A/R$  for  $R \approx 0$ . The regular field  $B_\phi$  should approach 0. In our numerical calculation, we do not impose such a strong condition as  $A/R \rightarrow 0$ . Therefore, there may be cusps on the  $Z$ -axis. Similarly, the  $B_Z$  field may be singular on the  $Z$ -axis. We set the boundary condition as  $\Phi = 0$  on the axis and numerically confirmed that  $\partial_R \Phi \approx 0$ , but there is no need for the smoothness of the numerical value  $B_Z = \partial_R \Phi / R$  near  $R = 0$ . Our numerical results show that there is possibly singular behavior of physical quantities,  $B_R$  near  $Z = 0$ , and  $B_\phi$  and  $B_Z$  near  $R \approx 0$ , but we need more precise calculations to reach a definite conclusion.

In Fig. 4, we show the ratio of the toroidal to poloidal components of the magnetic field,  $B_\phi / (B_R^2 + B_Z^2)^{1/2} \equiv B_t / B_p$ . Regarding the split-monopole field, the toroidal component gradually increases with  $R$  and dominates completely for  $R > R_{LC}$ . It also can be seen from our result that the toroidal field dominates, but not as strongly, in the exterior of the light cylinder.

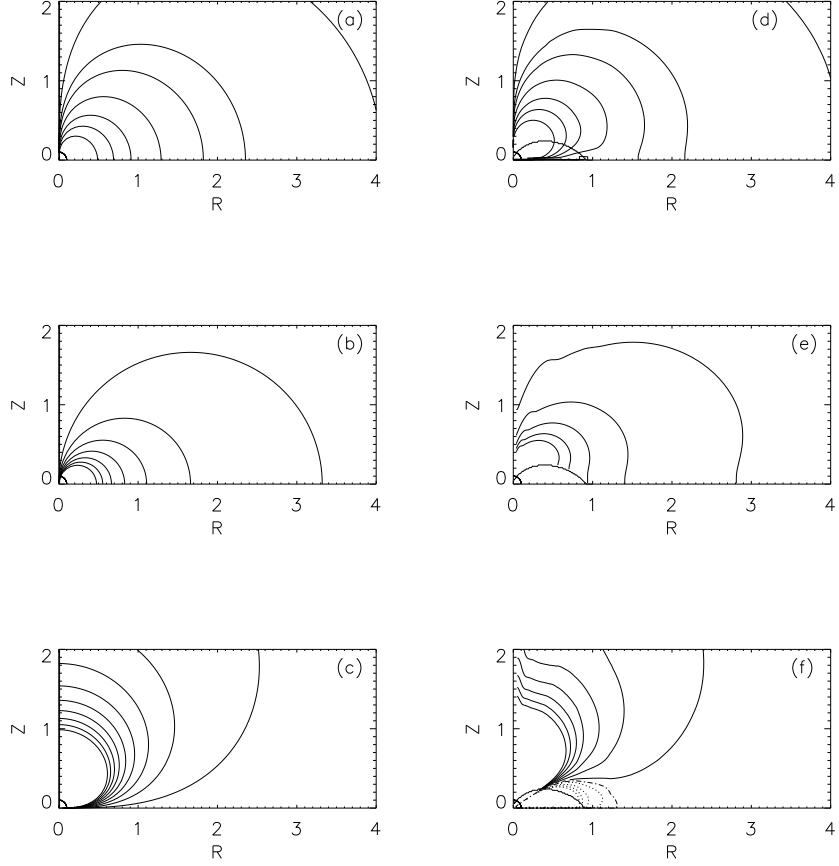


Fig. 3. Contours of the magnetic field strength for each component of the split-monopole field (a)-(c) and our numerical results (d)-(f). (a) The solid curves correspond to  $B_R = 7.0, 3.5, 2.0, 1.0, 0.5, 0.3$  and  $0.1B_o \equiv m/R_{LC}^3$ . (b) The solid curves correspond to  $B_\phi = -3.5, -3.0, -2.5, -2.0, -1.5, -1.0$  and  $-0.5B_o$ . (c) The solid curves correspond to  $B_Z = 1.7, 1.5, 1.3, 1.1, 0.9, 0.7, 0.5, 0.3$  and  $0.1B_o$ . (d) The solid curves correspond to  $B_R = 7.0, 3.5, 2.0, 1.0, 0.5, 0.3$  and  $0.1B_o$ . (e) The solid curves correspond to  $B_\phi = -2.5, -2.0, -1.5, -1.0$  and  $-0.5B_o$ . (f) The solid curves correspond to  $B_Z = 1.3, 1.1, 0.9, 0.7, 0.5, 0.3$  and  $0.1B_o$ , while dotted curves show outwardly  $B_Z = -0.7, -0.5, -0.3$  and  $-0.1B_o$ . The null line, along which  $B_Z = 0$ , is indicated by the dotted-dash curve.

#### 4.2. Drift velocity

The components of the drift velocity (2.2) are explicitly given by

$$\vec{v}_\perp = \left( -\frac{R\Omega}{B^2} B_R B_\phi, \frac{R\Omega}{B^2} (B_R^2 + B_Z^2), -\frac{R\Omega}{B^2} B_Z B_\phi \right). \quad (4.1)$$

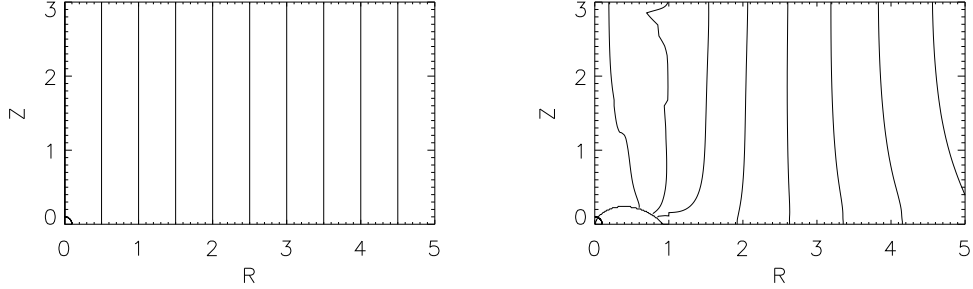


Fig. 4. Contours of the ratio of the toroidal to poloidal components of the magnetic field. The split-monopole solution is shown in the left panel and our result is shown in the right panel. The contour level increases from  $B_t/B_p = 0.5$  (innermost) at intervals of 0.5. The magnitude of the toroidal component exceeds that of the poloidal component beyond the light cylinder in both solutions.

The absolute magnitude is

$$v_{\perp} = R\Omega \frac{(B_R^2 + B_Z^2)^{1/2}}{(B_R^2 + B_{\phi}^2 + B_Z^2)^{1/2}} = R\Omega \frac{B_p}{(B_t^2 + B_p^2)^{1/2}}. \quad (4.2)$$

It is clear that the condition  $v_{\perp} \leq c$  holds inside the light cylinder. However, this condition is not guaranteed outside the light cylinder, and whether or not it holds depends significantly on the magnetic field configuration. Indeed, this condition holds everywhere for the magnetic field of the split-monopole, as shown in the appendix. In Fig. 5, we show the drift velocity  $v_{\perp}$  calculated from the CKF solution. The numerical result shows that  $v_{\perp} < 0.8c$  within the light cylinder and that the value  $v_{\perp}$  gradually increases with  $R$ . The drift velocity exceeds the light speed for  $R \gtrsim 3R_{LC}$ . This violation is clear, especially for small  $Z$ . The condition  $v_{\perp} \leq c$  means that the toroidal magnetic field should dominate for  $B_{\phi}^2/(B_R^2 + B_Z^2) \geq (R/R_{LC})^2 - 1$ , from Eq. (4.2). The ratio of the toroidal to poloidal components,  $B_{\phi}/(B_R^2 + B_Z^2)^{1/2}$ , increases with  $R$ , but the dependence is not as steep as for the split-monopole field. This difference leads to the violation of causality, i.e.  $v_{\perp} \geq c$  in the CKF solution, but no violation in the split-monopole case. It is thus seen that the applicable range of the CKF solution is limited within a few times the size of the light cylinder.

One may expect the breakdown of the drift approximation, as suggested in the literature,<sup>13)</sup> but it should be noted that the breakdown depends significantly on the adopted electro-magnetic fields. A counterexample is the split-monopole case. In this case, the drift approximation holds everywhere. The breakdown of the drift approximation is likely to occur outside the light cylinder for most electro-magnetic fields. In general, the location of the breakdown is not known *a priori*. The drift velocity cannot exceed the light velocity in a realistic situation. The inertial term gradually prevents the increase of the drift velocity as a particle moves away from a star. The magnetic field near a star is strong enough that the inertial term of the

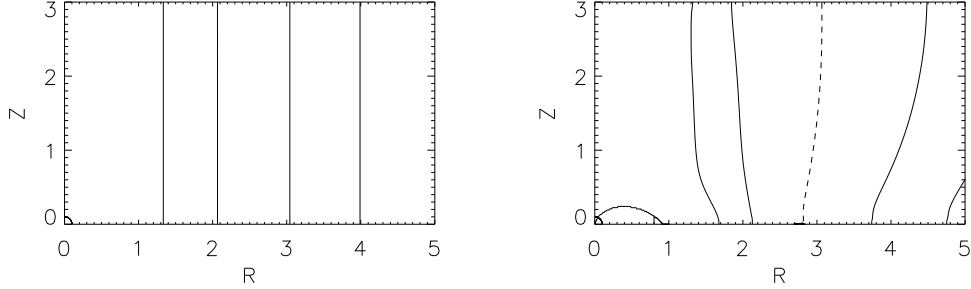


Fig. 5. Contours of the drift velocity for the split-monopole solution and our numerical results. The solid lines in the left panel indicate  $|v_{\perp}| = 0.8, 0.9, 0.95$  and  $0.97 c$ . The drift velocity of our result is shown in right-hand panel for the cases  $|v_{\perp}| = 0.8, 0.9, 1.1$  and  $1.2c$  (solid), and  $|v_{\perp}| = 1.0c$  (dotted).

particle can be ignored, but it decreases with the distance from the star. For this reason, the inertial term can no longer be ignored beyond a certain distance. This is a general picture, but the position beyond which the inertial term cannot be ignored depends strongly on the magnetic field configuration. In this paper, we have for the first time elucidated the properties of electro-magnetic fields described by the CKF solution and the drawbacks of the solution.

### §5. Remarks

In this paper, we have explored the axially symmetric magnetosphere around an aligned rotating dipole field. The ideal MHD and force-free conditions are satisfied everywhere by assuming a sufficient charge density. The electro-magnetic structure can be determined using the so-called pulsar equation, which is a coupled equation for  $\Phi$  and  $A$ . Some authors have examined some special cases in the past, e.g. that in which  $A$  is constant,<sup>17)</sup> linear in  $\Phi$ ,<sup>18)</sup> and quadratic in  $\Phi$ .<sup>9)</sup> However, these do not correspond to realistic situations. A new numerical solution reported by Contopoulos et al.<sup>15)</sup> seems to be promising. That solution may be useful as a starting point for a more realistic pulsar magnetosphere. From this point of view, we have examined the magnetic field and drift velocity in detail.

The overall global structure of the magnetosphere we have studied, is quite similar to that of a split-monopole field. Some difference in the current distribution  $A$  appears in regions corresponding to the case in which the field lines extend above the equatorial plane. A modification is necessary to connect the inner dipole-like field with the outer monopole-like field. This causes return currents, although the total amount of such currents is insufficient to realize current closure. For this reason a current sheet is required in the magnetosphere. Our result also shows the breakdown of the drift approximation beyond a few times the size of the light cylinder, and this result may modify the understanding regarding the CKF solution proposed in

Ref. 16). In that work, it was shown that the Lorentz factor of the outflowing plasma increases linearly with the distance from a neutron star. Therefore, at a large distance,  $R \sim 10^3 R_{LC}$ , the inertial term can no longer be ignored (i.e., the force-free condition breaks down), whereas our numerical calculation shows that the validity of the CKF solution is limited within a short distance  $\sim 3R_{LC}$ . Therefore some assumptions used in this calculation should incorporate the effects of a non-ideal MHD or the inertia of the particles in order to obtain a more realistic solution (e.g., see Ref. 4)).

### Acknowledgements

This work was supported in part by a Grant-in-Aid for Scientific Research (No. 14047215) from the Japanese Ministry of Education, Culture, Sports, Science and Technology.

### Appendix: Split-monopole solution

In this appendix, we consider the physical structure represented by the split-monopole solution. It may be useful to compare this explanation with the CKF solution. As noted by CKF, their solution asymptotically approaches the split-monopole solution.

When the function  $A$  is quadric in  $\Phi$ , the resultant magnetic field corresponds to the magnetic monopole solution. The solution of Eq. (2.8) can be explicitly written as

$$\Phi = q \left( 1 - \frac{Z}{(R^2 + Z^2)^{1/2}} \right), \quad (5.1)$$

$$A = -\frac{\Omega\Phi}{c} \left( 2 - \frac{\Phi}{q} \right), \quad (5.2)$$

where  $q$  is related to the monopole charge. This fact is easily checked by calculating the magnetic field given as

$$(B_R, B_\phi, B_Z) = \left( \frac{qR}{(R^2 + Z^2)^{3/2}}, -\frac{q\Omega R}{c(R^2 + Z^2)}, \frac{qZ}{(R^2 + Z^2)^{3/2}} \right). \quad (5.3)$$

The poloidal component of magnetic field ( $B_R, B_Z$ ) is always radial. This poloidal field dominates near the origin. By contrast, the toroidal field dominates across the light cylinder; that is,  $B_\phi > B_p = (B_R^2 + B_Z^2)^{1/2}$  for  $R > c/\Omega$ . In this way, this monopole solution represents a smooth transition of the magnetic field through the light cylinder. It may be helpful in obtaining physical understanding to calculate the current flow,

$$(j_R, j_\phi, j_Z) = \frac{q\Omega}{2\pi c} \left( \frac{RZ}{(R^2 + Z^2)^2}, 0, \frac{Z^2}{(R^2 + Z^2)^2} \right). \quad (5.4)$$

The current flow is purely poloidal and out-flowing, i.e.  $J > 0$ . This current gradually enhances the toroidal magnetic field  $B_\phi$ , which dominates outside the light cylinder.

The drift velocity is given by

$$(v_R, v_\phi, v_Z) = \frac{c\beta}{(1 + \beta^2)} \left( \frac{R\beta}{(R^2 + Z^2)^{1/2}}, 1, \frac{Z\beta}{(R^2 + Z^2)^{1/2}} \right). \quad (5.5)$$

It is easily verified that  $v_\perp \leq 1$  everywhere. This drift velocity asymptotically approaches the light speed as  $R \rightarrow \infty$ .

On the basis of the above consideration, there seems to be no problem with the monopole solution, except that it may not exist in nature. No monopole has yet been discovered in nature, and so this solution is used only for, e.g., upper hemisphere with  $+q$  and the lower hemisphere with  $-q$ . Combining these two solutions with opposite charge, the so-called split-monopole solution is sometimes used for physical analysis, e.g., in Ref. 10). In that case, the particle velocity of consistent flow is  $c$  everywhere.

### References

- 1) P. Goldreich and W. H. Julian, *Astrophys. J.* **157** (1969), 869.
- 2) J. P. Ostriker and J. E. Gunn, *Astrophys. J.* **157** (1969), 1395.
- 3) M. J. Rees and J. E. Gunn, *Mon. Not. R. Astron. Soc.* **167** (1974), 1.
- 4) L. Mestel and S. Shibata, *Mon. Not. R. Astron. Soc.* **271** (1994), 621.
- 5) F. V. Coroniti, *Astrophys. J.* **349** (1990), 538.
- 6) Y. Lyubarsky and J. G. Kirk, *Astrophys. J. Lett.* **547** (2001), L437.
- 7) A. Melatos and D. B. Melrose, *Mon. Not. R. Astron. Soc.* **279** (1996), 1168.
- 8) M. C. Begelman, *Astrophys. J.* **493** (1998), 291.
- 9) F. C. Michel, *Astrophys. J.* **158** (1969), 727.
- 10) F. C. Michel, *Astrophys. J. Lett.* **180** (1973), L133.
- 11) S. V. Bogovalov, *Astron. Astrophys.* **349** (1999), 1017.
- 12) F. C. Michel, *Theory of Neutron Star Magnetospheres* (The University of Chicago Press, Chicago and London, 1991).
- 13) V. S. Beskin, A. V. Gurevich and Ya. N. Istomin, *Physics of the Pulsar Magnetosphere* (Cambridge University Press, Cambridge, 1993).
- 14) V. S. Beskin, *Phys. Uspekhi* **40** (1997), 659.
- 15) I. Contopoulos, D. Kazanas and C. Fendt, *Astrophys. J.* **511** (1999), 351.
- 16) I. Contopoulos and D. Kazanas, *Astrophys. J.* **566** (2002), 336.
- 17) F. C. Michel, *Astrophys. J.* **180** (1973), 207.
- 18) E. T. Scharlemann and R. V. Wagoner, *Astrophys. J.* **182** (1973), 951.